Article

Enhancing Oxygen-Dissolving Capacity of Rotary Drum Food Waste Composting: Tumbling Process Optimization and Experimental Validation with Discrete and Finite Element Methods

Jufei Wang [1,2], Xueru Zhu [2,3], Zhenming Zhu [2,3], Chao Li [2,3], Xuesong Peng [1], Shilong Qiu [2,3,4], Jinbo Ren [1], Xinhui Wu [1], Samuel Mbugua Nyambura [2,3], Hua Li [2,3,*] and Shuhe Zheng [1,*]

[1] College of Mechanical and Electrical Engineering, Fujian Agriculture and Forestry University, Fuzhou 350002, China; jufei_wang@fafu.edu.cn (J.W.)
[2] College of Engineering, Nanjing Agricultural University, Nanjing 210031, China
[3] Key Laboratory of Intelligent Agricultural Equipment in Jiangsu Province, Nanjing 210031, China
[4] College of Mechanical and Electrical Engineering, Xinjiang Agricultural University, Urumqi 830052, China
* Correspondence: lihua@njau.edu.cn (H.L.); zsh@fafu.edu.cn (S.Z.)

Abstract: An optimized tumbling process can significantly improve the oxygen dissolving capacity of composting and fertilizer quality: by increasing the fluffiness of the lower layer of the pile, localized anaerobic fermentation can be avoided, thereby enhancing compost quality. This paper presents a method for improving the oxygen dissolving capacity of rotary drum food waste composting through a combination of simulation optimization and experimental validation. First, the discrete element method was used to optimize the key parameters of the tumbling process. The response surface method was then employed to analyze the composting test results and determine the optimal conditions. To ensure the reliability of the equipment under this method, failure risk analysis was conducted using the finite element method. The simulation optimization results showed that with a rotary drum reactor speed of 3.5 r/min, a horizontal angle of inclination of 2.5°, a mixing blade angle of inclination of 43°, and a blade pitch of 580 mm, the fluffiness of the lower layer of the pile increased by 8.515%, achieving the best tumbling and indirectly enhancing oxygen dissolving capacity. The maximum deformation of the load-bearing components was only 0.0548 mm, and the minimum safety factor was 4.408 (≥1 is considered safe). A 14-day composting experiment was conducted to validate the optimized parameters. The results showed that the maximum temperature of the compost pile reached 68.34 °C (lasting 7 days), with the pH, moisture content, C/N ratio, humus substances, humic acid, and fulvic acid contents of the fertilizer all meeting or exceeding the levels recommended by Chinese national standards. These findings indicate that the optimized tumbling device effectively improved the stability and dissolved oxygen efficiency of food waste composting, providing valuable practical insights and a research foundation for enhancing oxygen efficiency in the composting of other organic wastes.

Keywords: food waste; composting; rotary drum reactor; discrete element method; finite element method

1. Introduction

Food waste (FW) is not only linked to food security and resource wastage but also exerts significant pressure on combating climate change. According to the recently published Food Waste Index Report 2021 by the United Nations Environment Programme (UNEP), it is projected that globally, 931 million tons of food was discarded globally in 2019, constituting 17% of the total food available to consumers [1]. In China, the annual FW amounts to as much as 91.6 million tons, resulting in approximately 1.1 billion tons of greenhouse gas emissions [2]. Reducing the greenhouse gas emissions caused by FW is one of the most important pathways for China to achieve its carbon peaking and carbon

neutrality goals, thereby underscoring its importance. As a renewable resource, FW has significant utilization potential, with various technologies being employed for its treatment and utilization [3]. Among these technologies is the production of organic fertilizer based on FW, which is referred to as aerobic composting technology. Aerobic composting involves leveraging naturally occurring microorganisms that exist widely in nature to facilitate the biochemical process of converting degradable organic matter in solid waste into stable humus under controlled conditions, and it is mainly categorized into aerobic static composting and aerobic dynamic composting [4]. Continuous aerobic dynamic composting represents a dynamic secondary fermentation technology with a shorter fermentation period. Compared to other composting methods, continuous aerobic dynamic composting technology demonstrates superior economic benefits [5].

A rotary drum operates in continuous feeding mode [6] and is widely employed in continuous aerobic dynamic composting procedures. In this system, the materials are continuously turned in the drum to enhance pile porosity, thereby facilitating oxygenation and dewatering. Utilizing the rotary drum reactor effectively reduces the fermentation period, which is crucial for cost savings and enhancing processing capacity [7]. In recent years, it has garnered significant attention from both domestic and international research institutions and enterprises. For instance, Rodríguez et al. utilized a medium-sized rotary drum composting reactor to investigate the impact of tumbling frequency, oxygen content, type of expander, and sludge/expander mixing ratio on sludge composting, aiming to optimize the high-temperature phase and shorten the composting time. Their findings demonstrated that the optimization of the process variables and the reactor design effectively prolongs the thermophilic phase of the composting procedure and shortens fermentation time [8].

To explore the key factors influencing composting stability under different carbon to nitrogen (C/N) ratios and the dynamic organic matter decomposition process during composting, Nayak et al. analyzed the mixed composting of sludge, cow dung, and wood chips using a drum composting reactor. Stability and kinetic analyses of the composting and organic matter decomposition procedures were conducted. However, their study lacked the optimization of other key process parameters [9]. Sayara et al. developed a decentralized composting system for household waste treatment to address issues related to large-scale waste production and the inconvenient treatment of municipal solid waste [7]. A rotary drum composting reactor for organic waste composting was used to investigate the effects of different material types and different mixing ratios on composting equipment performance, which demonstrated enhanced efficiency in household organic waste treatment, yet their study offered limited discussion on improving dissolved oxygen efficiency and fertilizer quality during the composting process [7].

As the central component of a compost reactor, the tumbling device not only facilitates material tumbling and movement during composting but also assists the ventilation system in enhancing the pile dissolved oxygen efficiency (DOE). Selecting the appropriate tumbling process parameters can significantly improve composting stability and reduce energy consumption during tumbling [10]. Current research mainly focuses on the interaction mechanism between the materials and tumbling devices during the tumbling processes, as demonstrated by Soysal [11]. To reduce the long time required for the compost tumbling procedure and the high energy consumption, the design of a tracked compost tumbler was proposed through a coupled multibody simulation and discrete element method (DEM) simulation to develop a new compost tumbler that can autonomously perform tumbling and stacking tasks. **However, this research primarily examined the mechanical interaction without a comprehensive investigation into optimizing the process parameters for different feedstocks** [12]. Prommuak et al. compared the effects of different tumbling methods (vertical tumbling device and horizontal tumbling device) on the composting maturity of FW. The results showed similar composting characteristics under both tumbling methods, with the horizontal tumbling device showing better composting stability. However, their research lacked a detailed exploration of how specific tumbling parameters affect composting outcomes [13]. Liu et al. proposed a variable intermittent tumbling strategy

based on different fermentation stages to mitigate issues such as prolonged fermentation and high energy consumption. Through the finite element method (FEM) simulation of the tumbling process, the effect of different tumbling strategies on anaerobic fermentation was explored. The results revealed improved energy utilization with the variable intermittent tumbling strategy compared to traditional methods. But, their study did not address the broader applicability of this strategy for different aerobic fermentation materials and conditions [14].

In summary, the rotary drum reactor has demonstrated superior composting effectiveness and efficiency in aerobic dynamic composting. A well-selected tumbling process can significantly enhance the tumbling performance of the reactor, thereby improving the pile DOE and compost stability. Therefore, it is particularly important to optimize the tumbling process to increase the oxygen dissolution efficiency in rotary drum food waste composting, thereby improving the performance of the rotary drum composting reactor and the quality of the compost product.

To address the challenge of improving composting efficiency, this paper presents an innovative approach for designing a tumbling device for a rotary drum composting reactor, aimed at enhancing the oxygen dissolution efficiency during food waste (FW) composting. Based on the practical requirements for compost mixing and transfer, a tumbling and aeration device featuring a removable structure, adjustable mixing blade tilt angle, and adjustable blade spacing—adaptable to the characteristics of the composting material—was designed to improve the aeration and oxygen dissolution during the composting process. The device was subsequently optimized using DEM to evaluate the effects of key parameters, such as drum speed (RS), horizontal tilt angle (RA), mixing blade inclination angle (BA), and blade pitch (BP), on compost fluffiness and aeration efficiency. Additionally, a failure risk analysis was conducted using FEM to ensure the structural integrity and operational reliability of the equipment. Finally, validation experiments on the optimal combination of process parameters were conducted through prototype testing, which included measurements of compost quality indicators (e.g., temperature, pH, moisture content, C/N ratio, and humus) to verify the effectiveness of the proposed design under real-world conditions. This integrated approach, combining discrete and finite element analyses with experimental validation, not only optimized the tumbling aeration process but also ensured the practical feasibility and reliability of the equipment, ultimately contributing to improved FW composting stability and efficiency.

The innovation of this study lies in its comprehensive investigation of the key factors influencing the material dynamics within a rotary drum composting reactor and their effects on FW compost quality. By systematically optimizing crucial parameters, this research aimed at maximizing pile fluffiness, thereby enhancing DOE and ultimately improving compost quality. Moreover, the integration of DEM and FEM was found to be an effective approach for optimizing design parameters and assessing the structural reliability of the tumbling device. This integrated methodology not only advances the design process but also provides a robust framework for future research on compost reactor optimization and performance improvement.

2. Materials and Methods

2.1. Composting Material

To make the compost tumbling simulation test more realistic, a homemade FW blend was prepared with a high-oil and -salt recipe [15]. The raw materials used to prepare the standardized FW sample were sourced from a farmer's market in Nanjing, China. The sample composition consisted of 41.08% rice (staple food), 11.32% meat (protein and fat), 28.30% cabbage (vegetables), 16.98% water, 2.23% condiments (salt, sugar, edible oil, and spices) [15], and 0.1% bacterial agent [16] (the compound bacterial agent used for composting was a mixture of *Bacillus subtilis* (Kunshan Shengan Biotechnology Co., Ltd, Kunshan, China), *Aspergillus oryzae* (Shandong Qilu Chemical Science and Technology Co., Ltd, Jinan, China), nitrogen-fixing bacteria (Shanghai Preservation and Storage Bio-Technology Center, No./Identification: SHMCC 72579, Shanghai, China), and aerobic
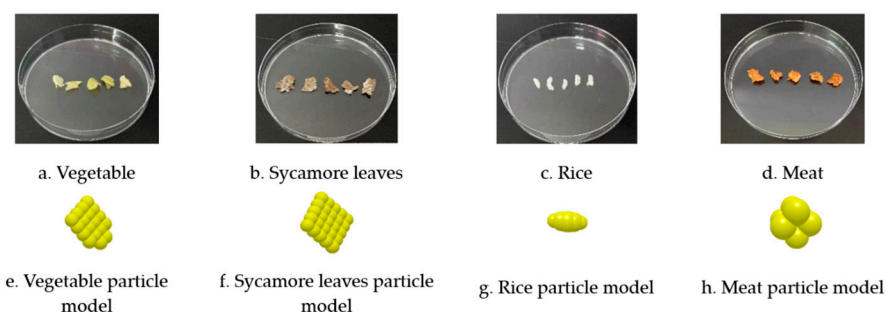
denitrifying bacteria (Guangzhou RanYi Bio-environmental Technology Co. Guangzhou, China) in a 1:1:1:1 mass ratio [17]). Sycamore leaves (SLs) collected from the campus of Nanjing Agricultural University were selected as the composting conditioner. To optimize composting performance, FW and SLs underwent shredding into particles approximately 10–15 mm in size using a shredder during the precomposting stage. Subsequently, FW and SLs were evenly mixed at a ratio of 3:1 (mass ratio) [18]. At this ratio, the initial C/N ratio of the compost feedstock was approximately 14.45, which is suitable for initiating the composting process and supporting microbial growth and proliferation [12,18]. The physicochemical properties of the composting material are shown in Table 1 [19].

Table 1. Basic physical and chemical properties of compost material.

Parameters	Food Waste	Sycamore Leaves
Moisture content (%)	81.40 ± 0.003	8.10 ± 0.004
Carbon/nitrogen ratio	5.60 ± 0.6	41 ± 3.2
Bulk density (kg/m^3)	1045 ± 25.43	168 ± 8.73
pH	8.24 ± 0.12	5.37 ± 0.05
Total carbon (%)	27.11 ± 0.5	46.28 ± 2.1
Total nitrogen (%)	4.84 ± 0.03	1.33 ± 0.02

To ensure the accuracy and reliability of the simulation data, a 28-day composting pretest was conducted. It was found that the composting process could be divided into three distinct stages: the warming stage, high-temperature stage, and cooling stage [20]. Initially, during the composting process, the material exhibited its highest water content, with microbial metabolism intensifying as composting progressed, leading to a gradual temperature increase within the compost pile. Concurrently, the evaporation of water and the decomposition of organic matter gradually reduced the viscosity of the pile [21,22]. Considering the correlation between the tumbling performance of the rotary drum reactor and pile viscosity, the material's viscosity peak was chosen as the focus of the compost tumbling simulation.

In this study, the resting angle of the compost material was measured daily from day 0 to day 9 using the fixed funnel method, with each test repeated three times. The average values recorded were 43.5 (day 0), 43.3 (day 1), 41.3 (day 2), 40.5 (day 3), 42.6 (day 4), 45.6 (day 5), 43.5 (day 6), 40.6 (day 7), 38.9 (day 8), and 37.6 (day 9). The compost from day 5, which exhibited the highest angle of repose and viscosity during the initial warming phase, was chosen as the representative material for the stirring experiments [15]. Three-dimensional laser scanning was used to capture the point cloud information of the compost feedstock [23], and a feedstock particle model was created using the multisphere method (MSM) and the fast filling technique, as shown in Figure 1 [24].

a. Vegetable   b. Sycamore leaves   c. Rice   d. Meat

e. Vegetable particle model   f. Sycamore leaves particle model   g. Rice particle model   h. Meat particle model

Figure 1. Physical picture and 3D particle pictures of compost materials.

Material density is critical in DEM simulations, as it directly influences particle interactions. As such, the approach used to determine material density has a significant impact on particle behavior. Similarly, the shear modulus, which defines material stiffness and deformation, is essential in discrete element simulations. The bulk density and shear

modulus were assessed and confirmed following the ASTM D2974-19 [25] and ASTM D7078-19 [26] standards, respectively. Poisson's ratio, indicating the volume change under compression and tension, was determined following ASTM E132-97 [27]. The physical parameters of the compost material are provided in Table 2.

Table 2. Physical parameters of the threshed simulation components.

| Object	Rice	Meats	Vegetables	Sycamore Leaves
Poisson's ratio	0.27	0.45	0.32	0.48
Density/kg·m^{-3}	1020.00	860.30	718.55	680.00
Shear modulus (G)/MPa	1.58	0.18	3.66	20.03

The coefficient of restitution, as well as the static and dynamic friction coefficients, are critical in discrete element modeling as they govern the behavior of particle collisions and energy dissipation during contact. The precise measurement of these properties is crucial for obtaining realistic simulation outcomes. The coefficient of restitution, along with the static and dynamic friction coefficients for particle collisions, were determined based on the ASTM D2632-15 and ASTM D1894-14 standards (Table 3) [28,29].

Table 3. Parameters of physical characteristics of mutual contact components.

Object	Rice–Rice	Rice–Meat	Rice–Leaves	Rice–Cabbage	Meat–Meat	Meat–Leaves	Meat–Cabbage	Leaves–Leaves	Leaves–Cabbage	Cabbage–Cabbage
Coefficient of restitution	0.09	0.11	0.11	0.13	0.10	0.11	0.12	0.15	0.11	0.14
Coefficient of static friction	1.51	1.45	0.98	1.04	1.35	0.95	1.11	0.68	0.81	0.82
Coefficient of rolling friction	0.01	0.01	0.01	0.02	0.01	0.01	0.01	0.01	0.01	0.01

2.2. Composting Setup

The composting device employed a self-developed rotary drum composting reactor, which comprised a frame, a drum, a tumbling device, an aeration system, a power device, an odor treatment device, and an accompanying control unit (Figure 2).
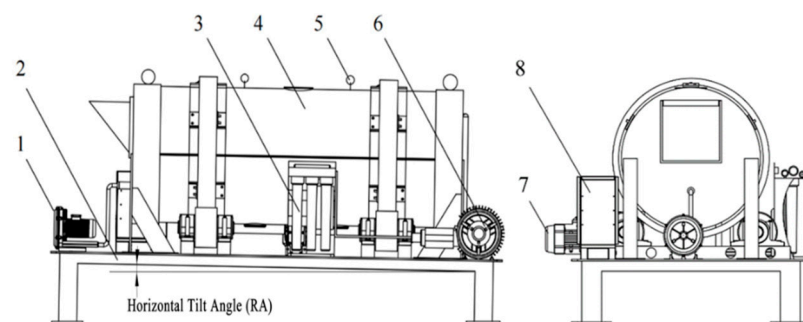

1. Aeration fan 2. Frame 3. Odor treatment device 4. Drum 5. Temperature and humidity sensor 6. Air pump 7. Motion device 8. Control module

Figure 2. Rotary composting reactor structure diagram.

Prior to initiating rotary drum operation, the material was introduced into the drum through a feeding port, and the drum was intermittently rotated as per composting requirements. During this process, the pile was turned and moved under the effect of the tumbling device, ensuring full exposure to air. Furthermore, sampling holes and temperature sensors were strategically positioned on the drum wall at the front, middle, and back to facilitate physical and chemical property determination after sampling and to monitor pile temperature parameters.

The drum reactor tumbling device comprised six hexagonal columns evenly spaced around the central axis of the drum and several sets of mixing blades distributed in a spiral, as shown in Figure 3. The tumbling device was primarily responsible for turning the pile and enhancing oxygenation, which accelerated the fermentation process. The installation angle and pitch layout of the mixing blade, as the key component of the tumbling device, significantly influenced pile mixing and oxygenation efficacy.
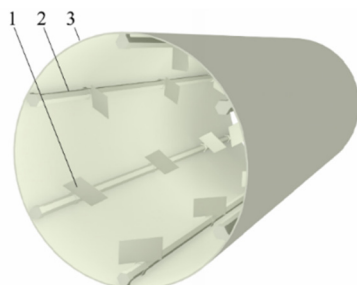
1. Mixing axes 2. Mixing blade 3. Drum

Figure 3. The drum reactor tumbling device diagram.

2.3. Experimental Method

2.3.1. Simulation Optimization Experiment

To illustrate the influence of the compost tumbling process parameters on the FW tumbling performance during the compost tumbling procedure and of the force of the blade on the tumbling procedure, this study introduced the concept of pile fluffiness, which determines the oxygen dissolving capacity of the pile; the fluffier the pile, the stronger the oxygen dissolving capacity [30].

A single-factor tumbling test was first carried out in this study using a standard FW sample at its peak viscosity stage as a simulated particle model. This test helped determine the range of parameters related to compost tumbling strength, which were then used for optimization in the subsequent tests. This simulation was performed using EDEM software (2020), which was specifically designed for the DEM analysis of bulk material behavior.

In the EDEM simulation, particles representing the FW sample were modeled with the appropriate material properties such as density, friction coefficients, and cohesion to reflect the characteristics of FW at its peak viscosity stage. The tumbling device's key parameters—drum speed (RS), horizontal tilt angle (RA), stirring blade tilt angle (BA), and blade pitch (BP)—were systematically adjusted in the software to observe their effects on compost motion and tumbling strength. The simulation allowed for the precise control and monitoring of particle interactions, enabling a detailed analysis of how these parameters influenced compost aeration and mixing.

According to previous studies, with RS (factor A) at 1~5 r/min [31,32], the pile tumbling effect is the best; RA (factor B) is usually 0.5~5° [33], and BA (factor C) is usually selected in the range of 15~60° [34,35]. As the drum mixing blades are distributed in a spiral pattern, BP (factor D) can be considered to be the spiral pitch. When the spiral pitch (S) and drum diameter (D) satisfy the condition S = 0.8D, the material movement effect is optimal. Thus, this relationship can be used to determine the range of BP [36]. The one-factor simulation test program for compost tumbling is shown in Table 4: the number of experimental groups was 20, and each group of experiments was repeated three times.

Table 4. Coupled single-factor simulation parameters.

No.	Factors	Values	Condition
1~5	Factor A (RS) (r/min)	1, 2, 3, 4, 5	3°, 30°, 480 mm
6~10	Factor B (RA) (°)	0, 1, 2, 3, 4	5 r/min, 30°, 480 mm
11~15	Factor C (BA) (°)	0, 15, 30, 45, 60,	5 r/min, 3, 480 mm
16~20	Factor D (BP) (mm)	240, 360, 480, 600, 720	5 r/min, 3°, 30°

The compost tumbling optimization experiment was designed using Design-Expert (Minneapolis, Minnesota) and the response surface methodology (RSM) to analyze the maximum and minimum RS, RA, BA, and BP values [37,38]. Subsequently, a Box–Behnken experimental design (BBD) method was employed to establish 27 sets of experimental schemes for FW compost tumbling optimization. The volumetric density (VD) of the pile served as the response index, with each experiment repeated 3 times. Multiple regression was conducted on the results to obtain the optimal combinations of compost tumbling parameters, thereby ensuring the reliability of the tumbling device in conjunction with the simulation verification.

The simulation time of the experiment was based on the drum rotation speed, which was set at one cycle, with the material generated from the particle factory simulated at a fixed rate (2.5 kg/s (staple food), 1.5 kg/s (protein and fat), 2 kg/s (vegetables), and 2 kg/s (sycamore leaves)). To precisely measure the VD of the pile during tumbling, the drum was split into top and bottom layers, and each layer was further divided into front, middle, and back sections. In EDEM's advanced postprocessing features, V_i represents the volume of the material in each section that can be fully output at various tumbling stages. The VD of the pile is calculated using the formula below:

$$V_A = (V_F + V_M + V_B)/3 \tag{1}$$

$$VD = (V_A/V) \times 100\% \tag{2}$$

In the formula,

V_A is the average volume of the pile in the bottom layer of the drum after tumbling, cm^3;

V_F, V_M, and V_B are the volume of the pile in the front, middle, and back sections of the drum after tumbling, cm^3, respectively;

VD is the rate of change in the volume of the pile in the bottom layer of the drum, %;

V is the volume of the pile in the bottom layer of the drum before tumbling, cm^3.

2.3.2. DEM–FEM Cosimulation for Optimizing Stirring and Tumbling Condition

In this study, the pressure and force data generated by the interactions between compost particles and the mixing blade during DEM simulations were used as the input for static analysis (FEM) [39]. This approach coupled DEM and FEM to simulate the stirring process, enabling the transfer of particle-induced forces from the DEM model to the FEM model for structural analysis [40].

In the cosimulation model of the stirring process combining DEM and FEM, the formula below illustrates the transfer of forces from the DEM simulation to the FEM analysis.

$$\left\{ \sum_{i=1}^{M} \left[\sum_{j=1}^{N} (k_n \delta_n n_{ij} + k_t \delta_t t_{ij}) + F_i^g \right] \right\} = [K][u] \tag{3}$$

where

k_n and k_t are the normal and tangential contact stiffness values in the DEM simulation, N/m;

δ_n and δ_t are the normal and tangential contact deformations, m;

n_{ij} and t_{ij} are the normal and tangential unit vectors;

F_i^g is the gravitational force acting on particle i, N;

M is the total number of particles in contact with the stirring device;

N is the total number of contacts per particle;

$[K]$ is the stiffness matrix in the FEM analysis, N/m;

$[u]$ is the displacement vector in the FEM analysis, m.

On the left side, the model calculates the forces from the DEM simulation, capturing the interactions between particles and the mixing blade. The right side of the model represents the FEM analysis, which depicts the relationship between external forces and nodal displacement. This enables the determination of displacements and internal pressures within the structure, forming the basis for structural risk assessments.

2.3.3. Verification Test

To verify the findings of the compost tumbling simulation optimization experiment, a verification test of the optimized compost tumbling design was carried out on the device as shown in Figure 4.
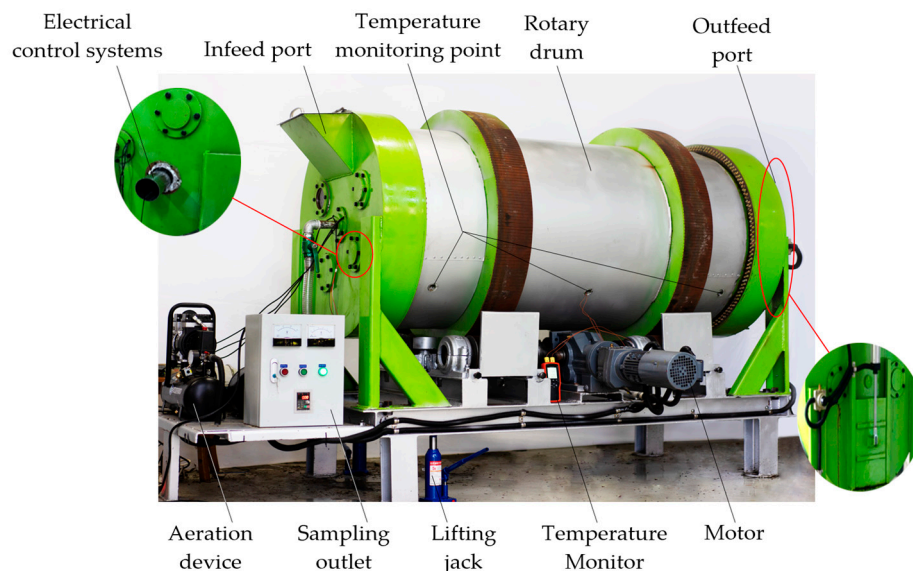
Figure 4. Real diagram of rotary composting reactor.

Following the results of the simulation compost tumbling optimization test, RS, RA, BA, and BP were individually set. Subsequently, the VD of the bottom layer of the pile in the composting drum after tumbling was calculated according to the following method: Firstly, we ensured the sampling area of the rotary drum reactor matched that of the simulation test. Sampling was carried out using the ring knife method before tumbling, and the pile volume was determined through the constant volume compression technique [41]. Considering that manual sampling had a degree of error, each area was sampled three times. V_{start} is the average value that was recorded as the volume of the pile before tumbling. Subsequently, the drive motor was activated, rotating the drum for one circle before the power was shut off. After tumbling, the pile volume was measured again using the ring knife method [12] and the constant volume compression method [41] and was recorded as the volume of the pile after tumbling, expressed as V_{end}.

Entering the above data into Formula (4) yielded the rate of change in the volume of the bottom layer of the pile in the drum after tumbling, VD:

$$VD = V_{end}/V_{start} \times 100\% \tag{4}$$

Considering the impact of tumbling on compost maturity and quality, secondary indicators including compost temperature, water content, pH, C/N ratio, humus content (humic substances, humic acid, and fulvic acid), and the seed germination index (GI) were selected to examine the tumbling effect. The temperature of the compost was collected using a K-type thermocouple temperature sensor, the moisture content was obtained using the drying method, the pH value was obtained by measuring the water extract of the compost material with a pH meter, and the C/N ratio was measured using an organic element analyzer. The humus contents including total humic substances (HS), humic acid (HA), and fulvic acid (FA) were examined according to the method reported by Albrecht [42]. GI was determined as follows: one or two pieces of qualitative filter paper were placed in a Petri dish, ten uniformly sized and full cucumber seeds were put evenly on it, 10 mL of sample extraction solution was added, the Petri dish was placed in an incubator at 25 °C ± 2 °C

for 48 h protected from light, and GI and shoot length were statistically measured. Finally, the GI value was calculated using Formula (5) [43].

$$\text{GI} = (A_1 \times A_2)/(B_1 \times B_2) \times 100\% \tag{5}$$

In the formula,

A_1 is the seed germination rate of organic fertilizer leachate, %;

A_2 is the average root length of seeds cultured in organic fertilizer leachate, mm;

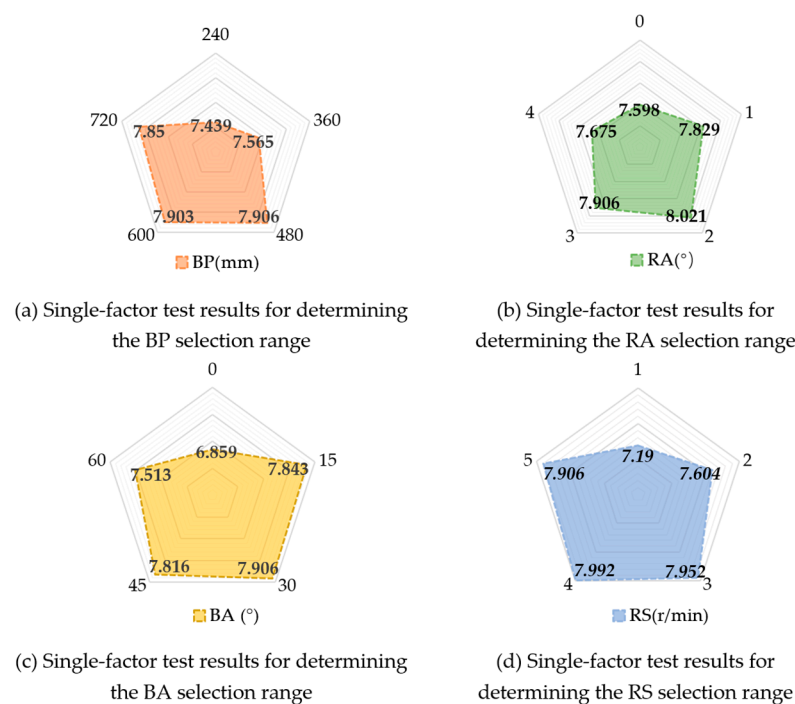B_1 is the seed germination rate of water, %;

B_2 is the average root length of seeds cultured in water, mm.

3. Results and Discussion

3.1. Simulation Optimization Test Results and Analysis

3.1.1. Single-Factor Test Results and Analysis

The results of the single-factor simulation experiment for compost tumbling (Figure 5a) show that when the BP is 240 mm and 480 mm, the VD is 7.439% and 7.906%, respectively; VD increases by 0.467%. When the BP is 600 mm, the VD is only 7.903%, which is almost the same as the VD (7.906%) when the BP is 480 mm. Therefore, the optimized range of the BP is 360 mm $\leq$ BP $\leq$ 600 mm.

(a) Single-factor test results for determining the BP selection range

(b) Single-factor test results for determining the RA selection range

(c) Single-factor test results for determining the BA selection range

(d) Single-factor test results for determining the RS selection range

Figure 5. Statistics of preliminary experimental results.

Figure 5b shows that when the RA increases from 0° to 2°, the VD increases gradually, and when the RA increases from 2° to 4°, the VD starts to decrease gradually; the maximum VD should be in the range of 1°~3°. Therefore, the optimized range is 1° $\leq$ RA $\leq$ 3°.

The results (Figure 5c) show that when the BA is 0°, the VD is 6.859%, which is at a lower level, and the VD values (7.843%, 7.816%) are similar when BA is 15° and 45°. Therefore, the optimized BA range should be 15° $\leq$ BA $\leq$ 45°.

Figure 5d shows that when the RS is 1 r/min, the VD is only 7.19%; at this time, the tumbling effect is poor. When the RS increases gradually, the VD also begins to rise gradually, and when the RS is located in the interval of 3~5 r/min, the VD reaches its maximum value. Therefore, the range of the RS in the optimized experimental parameters should be 3~5 r/min.

From the single-factor simulation test, the optimized ranges of the four key parameters that affect the compost tumbling performance are 360 mm $\leq$ BP $\leq$ 600 mm, $1° \leq$ RA $\leq 3°$, $15° \leq$ BA $\leq 45°$, and 3 r/min $\leq$ RS $\leq$ 5 r/min, as shown in Table 5.

Table 5. Simulated ranges of experimental factors.

Factor Level	RS (r/min)	RA (°)	BA (°)	BP (mm)
−1	3	1	15	360
0	4	2	30	480
1	5	3	45	600

3.1.2. Regression Model and ANOVA

The results of the compost tumbling optimization simulation experiment are shown in Table 6.

Table 6. Optimization simulation experimental design and results.

No.	RS (r/min)	RA (°)	BA (°)	BD (mm)	Max VD (%)
1	4	2	30	480	8.651
2	3	2	30	600	7.844
3	4	3	30	600	8.336
4	5	2	30	600	7.904
5	4	2	15	360	7.793
6	3	3	30	480	7.78
7	4	2	45	600	8.521
8	3	1	30	480	7.344
9	4	2	30	480	8.416
10	5	1	30	480	7.829
11	4	3	15	480	7.943
12	3	2	30	360	7.121
13	5	2	30	360	8.062
14	5	2	45	480	7.922
15	4	1	15	480	8.025
16	4	3	45	480	8.505
17	5	3	30	480	7.906
18	5	2	15	480	7.662
19	3	2	15	480	7.487
20	4	2	45	360	8.081
21	4	2	30	480	8.602
22	4	2	15	600	8.071
23	3	2	45	480	7.952
24	4	1	45	480	7.838
25	4	3	30	360	7.594
26	4	1	30	600	7.668
27	4	1	30	360	7.644

Multiple regression fitting calculations using the test results were performed using Design-Expert software (V12.0.3). These yielded a mathematical model relating the VD_{Max} and the test factors. This model was used to analyze and forecast the effects of various compost tumbling parameter combinations on the VD in FW compost tumbling simulation experiments [44]. As shown in Table 7, the mathematical model demonstrated a significance of less than 0.05, indicating that the model was statistically significant. The results of the simulation experiments showed that the response surface regression model had an insignificant ($p = 0.499 > 0.05$) misfit term, and the coefficient of variation (CV) = 1.77% < 10%. This suggested that nonexperimental factors had a minimal impact on the model's predictions, indicating strong model stability [45]. The model's correlation coefficient (R^2) was 0.936, indicating a strong fit between the model and actual experimental data, with approximately 93.6% of the actual test results predicted by the fitted model. The adjusted R^2 (adjusted

coefficient of determination) was 0.8614, which was close to R^2, suggesting that the model is both accurate and generalizable. Therefore, this model is a useful tool for analyzing and predicting the influence of different factors on the VD in optimization experiments of FW compost tumbling.

Table 7. Analysis of variance in test results.

| Source	Sum of Squares	df	Mean Square	F-Value	*p*-Value	Significance
Model	3.48	14	0.2483	12.54	<0.0001	***
A-RS	0.2573	1	0.2573	12.99	0.0036	**
B-RA	0.2454	1	0.2454	12.39	0.0042	**
C-BA	0.2815	1	0.2815	14.22	0.0027	**
D-BP	0.3499	1	0.3499	17.67	0.0012	**
AB	0.0322	1	0.0322	1.63	0.2262	/
AC	0.0105	1	0.0105	0.5306	0.4803	/
AD	0.194	1	0.194	9.8	0.0087	**
BC	0.1403	1	0.1403	7.08	0.0207	*
BD	0.1289	1	0.1289	6.51	0.0254	*
CD	0.0066	1	0.0066	0.3314	0.5755	/
A^2	1.58	1	1.58	79.87	<0.0001	***
B^2	0.6336	1	0.6336	32	0.0001	***
C^2	0.1563	1	0.1563	7.89	0.0158	*
D^2	0.5335	1	0.5335	26.95	0.0002	***
Residual	0.2376	12	0.0198	-	-	-
Lack of Fit	0.2069	10	0.0207	1.35	0.4998	/
Pure Error	0.0307	2	0.0154	-	-	-
Cor Total	3.71	26	-	-	-	-

Note: *** Strongly significant ($p < 0.001$); ** highly significant ($p < 0.01$); * significant ($p < 0.05$); / not significant.

3.1.3. Regression Model Response Surface Analysis

The results of the ANOVA showed that the effects of factors A, B, C, D, AD, BC, BD, A^2, B^2, C^2, and D^2 in the objective function on the VD were all significant, and the order of significance of the effect of the four factors, namely, A, B, C, and D, on VD was D > C > A > B. To analyze the effects of the interaction factors on the VD, response surface analyses of the interaction factors AD, BC, and BD were conducted in this study using the control variable method. An RS of 4 r/min, an RA of 2°, a BA of 30°, and a BP of 480 mm were chosen as the median values of each influencing factor. Then, the RSM was used to handle the experimental data so as to obtain the response surface plots and contour plots of the VD with each interaction factor (Figure 6).

As shown in Figure 6a, the response surface of AD was curved with elliptical contour lines, and the interaction between RS and BP was highly significant ($p < 0.01$). When RA and BA were fixed (RA = 2°; BA = 30°), there was a parabolic relationship between RS and VD, and with the increase in RS, VD showed an initial increase, followed by a decrease, with a steeper overall trend. Similarly, as BP increased, VD displayed an initial increase followed by a decrease, albeit with a more moderate overall trend. The optimal tumbling effect (VD = 8.585%) was achieved when RS was approximately 4 r/min and BP was approximately 480 mm, whereas the smallest VD (7.155%) was observed at an RS of 3 r/min and a BP of 360 mm.

As shown in Figure 6b, the response surface of BC exhibited less curvature with elliptical contours, and the interaction between RA and BA was significant ($p < 0.05$). When RS and BP were fixed (RS = 4 r/min; BP = 480 mm), VD increased and then decreased with increasing RA, with a small change in amplitude, and VD increased gradually with increasing BA. The optimal tumbling was obtained at an RA of 2° and BA tended to 45° (VD = 8.638%), whereas the least effective tumbling occurred when RA tended to 3° and BA tended to 15° (VD = 7.838%).

(a) VD (A, 2°, 30°, D)

(b) VD (4r/min, B, C, 480mm)

(c) VD (4r/min, B, 30°, D)
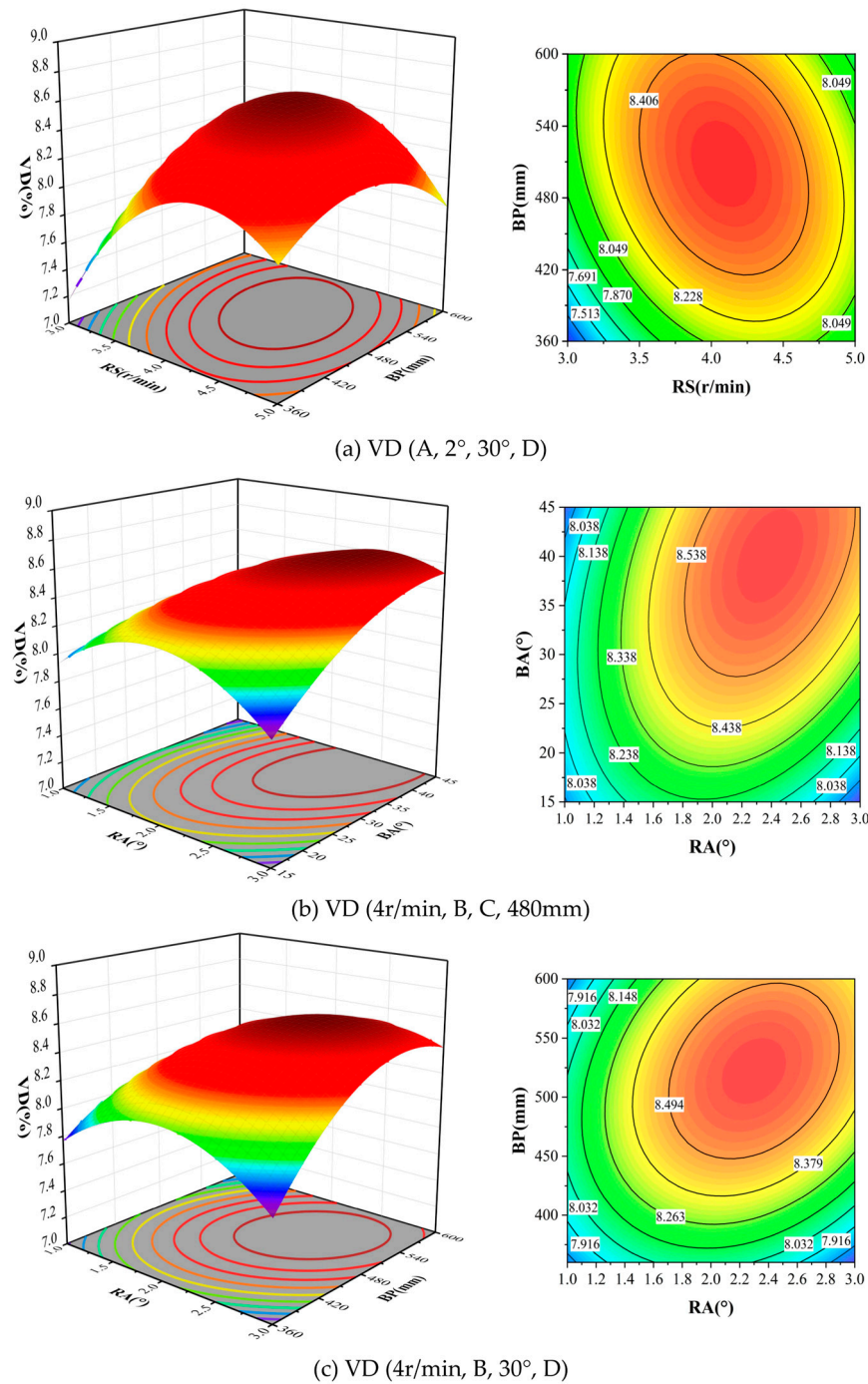
Figure 6. Response surface illustrations showing the interactions between different factors.

As shown in Figure 6c, the response surface of BD had a similar trend to that of BC: the contours were elliptical, and the interaction between BA and BP was significant ($p < 0.05$). When RS and BA were fixed (RS = 4 r/min, BA = 30°), VD increased and then decreased with the increase in RA. The tumbling effect was poor when RA was 3°; VD increased gradually with the increase in BP and began to decrease gradually when BP was close to 540 mm. The best tumbling effect was obtained when RA was 2° and BP was 540 mm, reaching 8.610%. When RA tended to 3° and BP tended to 360 mm, the VD value was the smallest at 7.685%.

Based on the above simulation optimization experimental results, the following conclusions were drawn:

Analyzing the microparticle motion and collisions shows that during the compost mixing process, microparticles are in constant motion and experience frequent collisions [46]. As the RS increases, the increased rotational speed leads to higher kinetic energy in the particles, resulting in more frequent collisions. These collisions facilitate greater dispersion and mixing of the particles, enhancing the oxygen transfer through the compost mass. For instance, at an RS of 4 r/min, the VD reached its maximum value of 8.585%, highlighting the crucial impact of particle movement and collisions during higher-speed stirring. Higher RS values promote greater particle agitation, preventing the formation of localized anaerobic zones by disrupting compacted areas, which allows for better air circulation and oxygen diffusion into the pile. An analysis of particle flow and alignment indicates that the RS significantly affects the movement and arrangement of particles in the rotary drum. At lower speeds, particles tend to accumulate in piles, which limits changes in the VD. In contrast, higher stirring speeds promote particle rearrangement and agitation [46], resulting in a boost in the VD. For instance, at an RS of 3 r/min, particles align more tightly, leading to a lower VD. However, at 4 r/min, the increased particle rearrangement contributes to a higher VD.

In addition to particle movement, interparticle friction plays a significant role in enhancing the overall composting process. As RA increases, friction between particles also increases, promoting more intensive interactions. These interactions lead to better mixing and the breakdown of larger clumps of compost material, further improving the contact surface between particles and oxygen. Taking inter-particle friction and forces into account, it can be hypothesized that increasing RS enhances the frictional forces between particles, thereby intensifying their interactions and subsequently increasing VD [47]. At the optimal BA, the angle of the blades enhances the tumbling effect by maximizing particle displacement and maintaining a balanced flow. This balance between agitation and particle realignment ensures that oxygen can efficiently dissolve throughout the compost. With RA maintained at 2.4°, VD gradually increased as BA increased. For example, at a BA of 45°, VD reached 8.638%, indicating that increased friction and force enhanced the particle interactions. This indicates the presence of an optimal point where stirring achieves maximum efficiency, resulting from a balanced interplay between particle friction and applied forces.

These findings demonstrate that the optimal composting performance, measured by the VD, is strongly influenced by key parameters such as the RS, BP, RA, and BA. The interaction between these parameters affects particle movement, alignment, and collision dynamics, which are critical for maximizing compost aeration and oxygen dissolution.

To further ensure the reliability and feasibility of the ANOVA model, we also investigated the reasons behind the nonsignificance of the interaction terms AB, AC, and CD to further validate the model's accuracy in reflecting the mechanism of the effects of the system's factors.

For AB, in the rotary drum composting process, RS directly influences the mixing frequency of the compost material, while RA determines the axial movement speed of the material within the drum. Given the high density of the food waste and sycamore leaf mixture before and after fermentation, the mixing frequency is more sensitive to changes in the RS. In this study, the variation in RA was relatively small, resulting in minimal vertical displacement changes in the center of gravity of the feedstock [32,34]. Consequently, the movement of the compost material within the drum was largely influenced by gravity and centrifugal force, making the combination of RS and RA independent in enhancing or inhibiting material fluffiness under the current experimental conditions. Thus, their interaction effect on VD was statistically nonsignificant.

For AC, in the drum, BA determines the sliding and flipping of the material along the blade, particularly affecting the microlevel mixing of the materials. Meanwhile, RS primarily impacts the overall circulation speed within the drum, having a more noticeable effect on the tumbling of heavier food waste. The variation in RS enhances the overall circulation rate on a macro scale [34], while the changes in BA are more associated with

localized, microlevel tumbling effects [7,24]. Therefore, the combination of RS and BA did not create a synergistic effect on the overall mixing efficiency.

For CD, BA and BP both play roles in the local tumbling and propulsion of the material. For denser food waste, BP significantly affects its axial movement path [11], while BA influences the tumbling intensity of the material [7]. Compared to the influence of BP on material tumbling, the macro effect produced by BA is relatively minor. This leads to overlapping and offset effects of the two factors on the fluffiness of the material heap, thereby weakening the interaction effect between BA and BP on the overall mixing efficiency [47]. Thus, the interaction between BA and BP did not significantly influence VD in the statistical analysis.
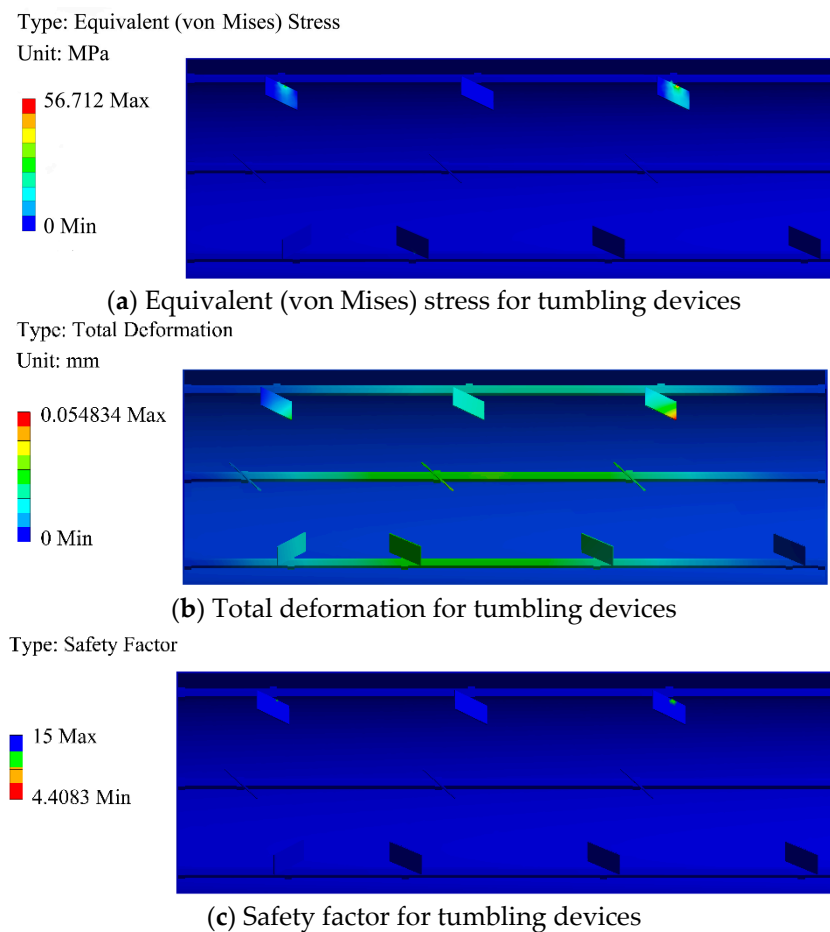
3.1.4. Failure Risk Analysis

The results of the ANOVA and response surface analysis (RSA) of the regression model showed that the optimal compost tumbling occurred at an RS of 3.95 r/min, an RA of 2.57°, a BA of 42.4°, and a BP of 540.3 mm, yielding a VD value of 8.699%. To verify the reliability of the compost tumbling device under these parameters, an FEM analysis of the tumbling device was carried out in this study using EDEM coupled with ANSYS to evaluate the equivalent total deformation and safety performance [47]. The data from EDEM were transferred to ANSYS Workbench, where a static structural analysis was performed to evaluate the device's mechanical behavior under operational conditions. The process involved coupling the discrete element simulation (DEM) and the finite element method (FEM) to assess both particle forces and structural response. Under the specified parameters, the tumbling device experienced a maximum compression force of 10.9 MPa when the drum was rotated to 247.2° (Figure 7).
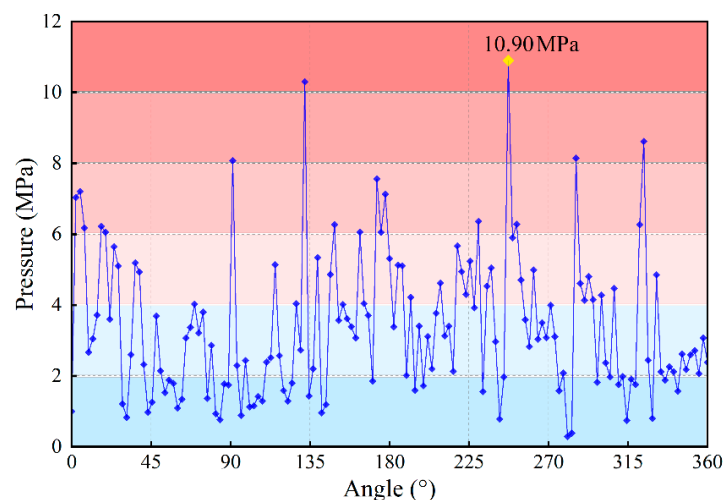
Figure 7. Pressure force diagram of stirring device at different angles.

Based on the results of the finite element analysis (FEA), the maximum strain experienced by the tumbling device at the maximum pressure (247.2°, 10.9 MPa) amounted to 56.712 MPa, which was mainly concentrated at the connection between the blade and the mixing axle (Figure 8a). The yield strength of the tumbling device (45# steel) was 355 Ma, which indicated that the structural strength of the tumbling device met the design requirements. Significantly, the point of maximum deformation often indicates the most likely site of damage [48]. It can be seen from Figure 8b that the deformation of the tumbling device mainly occurred on the blade, with the maximum deformation being only 0.0548 mm, which is negligible.

Type: Equivalent (von Mises) Stress
Unit: MPa

56.712 Max

0 Min

(**a**) Equivalent (von Mises) stress for tumbling devices

Type: Total Deformation
Unit: mm

0.054834 Max

0 Min

(**b**) Total deformation for tumbling devices

Type: Safety Factor

15 Max

4.4083 Min

(**c**) Safety factor for tumbling devices

Figure 8. Stress, strain, and safety factor diagrams for tumbling devices at maximum performance pressure.

Blade deformation and pressure variations can be influenced by changes in RA and BP, which directly affect VD. A larger BP tends to result in more significant pressure fluctuations, ultimately reducing VD. In the experiments, reducing the RA widened the variation range of the pressure on the blade, causing more deformation. For example, with a larger BP and a lower RA, the changes in pressure were minimal; but, adding RA or reducing BP obviously increased the variations in pressure, resulting in greater blade deformation. This suggests that excessive blade deformation adversely impacts mixing efficiency. Therefore, controlling blade deformation and pressure variations is essential for maintaining equipment stability and operational efficiency.

Furthermore, to assess the sensitivity of the tumbling device to breakage, a safety factor analysis was conducted. A safety factor exceeding one indicates safety, while less than one suggests danger [49]. The analysis of the pressure transfer and stress concentration shows that as RS increases, the pressure transfer within the compost material also intensifies. Under certain conditions, such as an RA of 2.5° and a BA of 42°, abrupt pressure drops may occur [50], resulting in an increase in VD. Sudden pressure surges in the compost feedstock could surpass the blade's tolerance limit, leading to potential fractures. As shown in Figure 8c, the location exhibiting the minimum safety factor aligned with the stress concentration zone, with a safety factor of 4.408, which indicated that the fracture damage risk of tumbling device during material tumbling was extremely low.

During the mixing and stirring process, changes in blade deformation and pressure influence the compost's fluffiness, while stress concentration and pressure transfer can lead to blade fractures, affecting the tumbling device's stability and efficiency.

3.2. Analysis of the Results of the Verification Test

3.2.1. Optimal Combination Validation Experiments

The results of the ANOVA and response surface analysis (RSA) of the regression model showed that the optimal compost tumbling occurred at an RS of 3.95 r/min, an RA of 2.57°, a BA of 42.4°, and a BP of 540.3 mm, yielding a VD value of 8.699%. However, for practical operational feasibility, these parameters were adjusted as follows: RS = 4 r/min; RA = 2.6°; BA = 42°; and BP = 540 mm. Prototype validation tests were conducted three times for this parameter combination, yielding an average actual VD of 8.515%.

The validation test yielded a relative error of 2.115% compared to the simulation analysis for VD (95% confidence interval, shown in Table 8). This consistency between the validation results and the regression model predictions confirms the reliability of the statistical model in optimizing composting conditions using food waste as the feedstock.

Table 8. Results of performance validation for optimal parameter combinations.

No.	RS (r/min)	RA (°)	BA (°)	BP (mm)	Max VD (%)
1					8.693
2	4	2.6	42	540	8.321
3					8.531
Average value	/	/	/	/	8.515
Error (%)	/	/	/	/	2.115

3.2.2. Physiochemical Properties

In order to further illustrate the effectiveness of the above design method and composting process and its effect on the quality of organic fertilizer, a 14-day composting experiment was conducted. The composting test results (Figure 9a) indicated a rising temperature trend in the pile until the sixth day of composting, followed by a decline. Specifically, the pile entered the high-temperature composting stage ($\geq$50 °C) on the third day and maintained this elevated temperature for 7 days. The pile reached its peak temperature (68.34 °C) on the sixth day of composting, and then gradually decreased until it approached ambient temperature. It is worth noting that odor production commenced after the compost entered the high-temperature stage, and this persisted until the sixth day. This was attributed to the elevated temperature and the diminishing nitrogen fixation effect of the material. In the composting procedure, nitrogen fixation typically relies on biological nitrogen fixation, which is a specific physiological function of nitrogen-fixing microorganisms. In this study, nitrogen fixation was facilitated by the nitrogen-fixing bacteria (genera such as *Azotobacter*, *Clostridium*, and *Klebsiella*) included in the compound bacterial agent, as described in Section 2 [51,52]. However, the nitrogen fixation activity pf these nitrogen-fixing microorganisms was limited [53]. When the pile temperature neared 70 °C, the activity of the nitrogen-fixing microorganisms was significantly diminished, thereby affecting nitrogen fixation [54]. Consequently, a substantial amount of nitrogen was lost from the pile in the form of ammonia, resulting in a pungent odor. This highlights the role of optimized tumbling in maintaining effective aeration during the high-temperature phase, which is crucial for nitrogen retention and overall compost quality.

As the raw material used was FW, its hydrolysis and acidification during transportation and storage resulted in a low initial pH [55]. From Figure 9b, it is evident that during the composting process, the pH value of the pile gradually increased. In the warming stage, the pH value of the pile ranged between 6.5 and 7.5, indicating weak acidity or neutrality. Upon entering the high-temperature period, there was a significant decrease in the pH value of the pile, which reached the lowest point on the third day of this stage. This decline was attributed to the rise in temperature, which fostered the rapid multiplication of acid-producing microorganisms (such as species from genera *Lactobacillus* and *Clostridium*) and the presence of organic acid precursors from plant-derived materials [52]. This resulted in

the accumulation of organic acids, followed by a reduction in pH [56], which was consistent with the temperature curve trend.
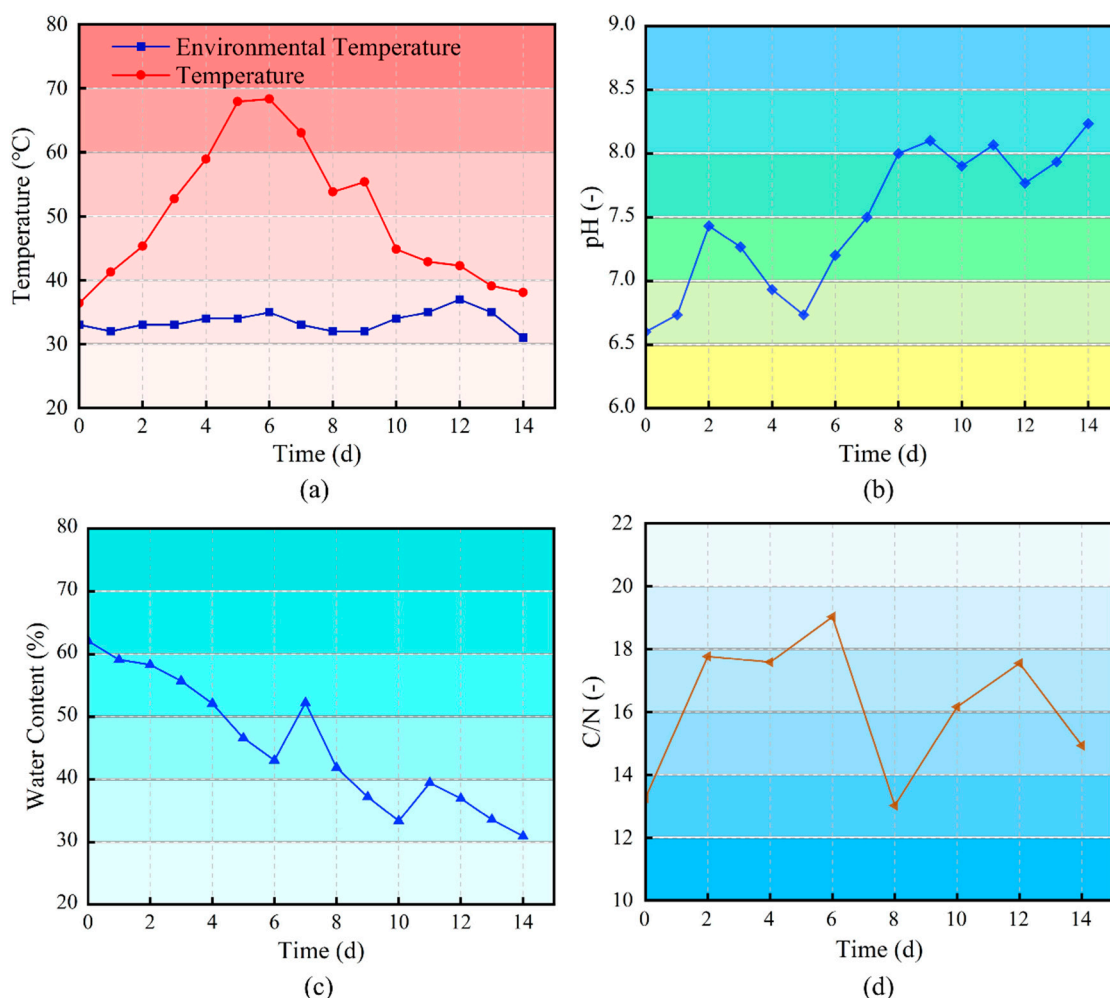
Figure 9. (**a**) Temperature, (**b**) matrix pH, (**c**) water content, and (**d**) C/N during composting.

These observations align with the results from the aeration and tumbling optimization study, as proper aeration facilitated by the optimized tumbling parameters helped with controlling pH fluctuations by providing sufficient oxygen for the microbial breakdown of organic acids, thereby supporting compost stability and quality improvement. As aerobic fermentation progressed, the organic acids and proteins in the pile were broken down by microorganisms, leading to a gradual pH increase to approximately 8.2. While an elevated pH can induce NH_3 volatilization due to the conversion of ammonium ions (NH_4^+) to ammonia gas (NH_3), the optimized tumbling and aeration parameters in this study helped control NH_3 loss by maintaining adequate oxygen levels for microbial activity and reducing ammonia emissions [53,57]. Consequently, the compost exhibited weak alkalinity at this stage [19], in line with national compost decomposition standards.

As depicted in Figure 9c, the water content of the compost pile decreased throughout the composting period. The decline in water content during the warming stage was slower, remaining above 55%. Upon entering the high-temperature period, the water content decreased rapidly. Notably, on the fifth day of the high-temperature stage, the water content of the pile appeared to increase. This increase was attributed to the condensation within the composting reactor. At elevated temperatures, the accelerated degradation of organic matter and the thermal expansion of water molecules [58] generated water vapor

within the pile (days 5–8). Due to incomplete discharge, some of this vapor condensed and flowed back into the pile, temporarily raising the water content [7].

This observation provides further evidence that the optimized tumbling significantly enhanced pile fluffiness, improving the aeration channels. Improved aeration directly contributed to more-effective moisture removal, especially during the high-temperature phase. With the gradual reduction in the pile temperature, the water content of the pile body decreased to nearly 30%. During this period, slight fluctuations in the water content occurred due to a decrease in temperature, causing the water vapor to condense on the drum wall and drip off.

The C/N ratio is an important indicator of compost maturity, with compost generally considered mature when the C/N ratio falls within 10–20 [59]. From Figure 9d, it can be observed that with an increase in the temperature, the C/N ratio gradually rose, which was consistent with the temperature trend. The high temperature led to the loss of nitrogen, which resulted in an increase in the C/N ratio. During the high-temperature phase, microbial activity intensifies, accelerating the breakdown of organic compounds. This rapid decomposition produces high levels of nitrogen volatilization, especially in the form of ammonia, due to the degradation of proteins and other nitrogen-containing compounds [57]. The resulting nitrogen loss was primarily responsible for the observed increase in the C/N ratio [53]. Upon entering the cooling stage, the C/N ratio initially decreased, then rose, before declining again. In the cooling stage, microbial activity slows, which reduces nitrogen volatilization and allows nitrogen to stabilize within the compost feedstock [17]. The initial decrease in the C/N ratio reflects a balance between carbon decomposition and nitrogen retention [60]. However, the subsequent increase can be attributed to the further breakdown of the remaining organic matter, which concentrates carbon relative to nitrogen as nitrogen losses stabilize [60]. As the compost reaches maturity, both carbon and nitrogen levels stabilize, leading to a final decrease in the C/N ratio as the compost material becomes more homogeneous and decomposed.

This observation proves that the optimized tumbling process helped to evenly distribute oxygen and enhance microbial activity, thus supporting a more stable C/N ratio trend. It is noteworthy that this fluctuation pattern in the C/N ratio differs from the findings of previous researchers [61], who observed a continuous decrease in the C/N ratio to within a stable interval during organic waste composting. The inconsistency may have originated from the low organic carbon content in the pile, which accelerated the biodegradation of organic nitrogen compounds during composting [19].

3.2.3. Biochemical Properties

The humus content change curves of the composting process (Figure 10a) show that the contents of HS and HA exhibited a decreasing trend before the eighth day, followed by a gradual increase. Conversely, the content of FA showed a continuous decrease throughout the fermentation process. Since the change trends in the HS and HA contents were not pronounced during the initial composting period, additional trend data on contents of HS, HA, and FA in the pile from the 14th to the 20th days were included to supplement the analysis. Due to the initially high and unstable contents of HA and FA, some of the precursors of HS were decomposed via microbial metabolism at the onset of composting, resulting in significant decreases in HA and FA [62]. Notably, sharp increases in both HS and HA was observed on the fourth to sixth days of composting, which was attributed to the rapid proliferation of acid-producing microorganisms (such as *Lactobacillus* spp., and *Clostridium* spp.), leading to the accumulation of organic acids [51,63].

This finding suggests that the rapid proliferation of microorganisms was facilitated by the optimized tumbling process, which ensured adequate pile fluffiness and oxygen availability, thereby creating favorable conditions for humus production. Specifically, the increased microbial activity and effective oxygen transfer contributed to the production of intermediate organic acids, promoting humus synthesis.
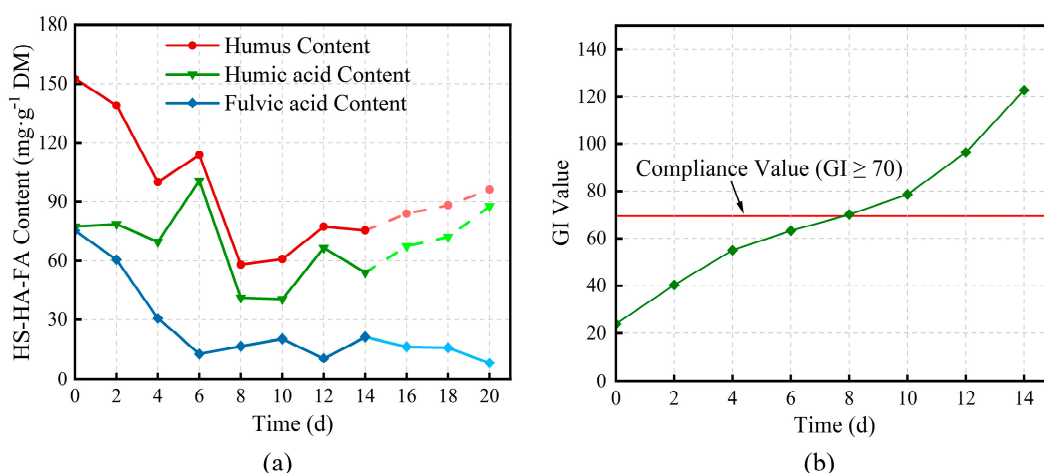
Figure 10. (**a**) Variations in the contents of total HS, HA, and FA; (**b**) GI value during composting.

Subsequently, after the eighth day, a substantial amount of organic matter (including lignocellulose and macronutrients) was degraded into HS precursors such as polyphenols, polysaccharides, and amino acids, thereby promoting HS synthesis. The gradual increases in HS and HA also underscore the role of effective aeration, which was achieved through the optimal tumbling process, in sustaining microbial activity and the synthesis of stable organic matter. Additionally, FA can undergo polymerization with aromatic-rich carbons to form stabilized HA [64], thereby contributing to the gradual increases in HS and HA.

GI is a widely accepted index for evaluating the toxicity and maturity of compost [65]. The most recent Chinese agricultural industry standard, 'Technical Specifications for animal manure composting' (NY3442-2019) [65], and the latest organic fertilizer standard (NY525-2021) [65] both stipulate that mature compost should have a GI of more than 70%. The results presented in Figure 10b show that as aerobic fermentation progressed, material decomposition increased, leading to a rise in the GI. The compost maturity requirements were met on the 8th day of composting, reaching 123% on the 14th day.

These observations align with the conclusions from the aeration and tumbling studies, supporting the effectiveness of the optimized tumbling aeration process.

4. Conclusions

This study developed an optimized tumbling process for a rotary drum compost reactor aimed at improving the oxygen dissolving capacity in food waste composting. By optimizing key parameters, including the RS, RA, BA, and BP, the process was enhanced to increase pile fluffiness, thereby avoiding localized anaerobic conditions and improving compost quality. DEM was used to determine the optimal parameter values, while RSA identified the most favorable conditions for composting performance. To ensure the reliability of the proposed process, a failure risk analysis was conducted using FEM, which confirmed strong structural integrity with minimal deformation (with a maximum deformation of 0.0548 mm and a minimum safety factor of 4.408). The optimal tumbling parameters (RS: 4 r/min; RA: 2.6°; BA: 42°; BP: 540 mm) resulted in an increased fluffiness of 8.515%, achieving the best tumbling effect. The results of validation tests showed close agreement with the simulation results, with a maximum pile temperature of 68.34 °C sustained for 7 days in the composting experiments. The final compost had a pH of 8.2, a moisture content reduced to 30.94%, and a C/N ratio stabilized at around 15. The humus substance, humic acid, and fulvic acid contents were 75.4 mg·g^{-1}, 54 mg·g^{-1}, and 21.4 mg·g^{-1}, respectively, all surpassing national standards. Additionally, the GI reached 123%, indicating full decomposition and compost maturity. These findings demonstrate that the optimized tumbling process effectively improved the oxygen dissolving capacity and compost stability, offering valuable insights for similar composting processes aimed at enhancing oxygen efficiency and product quality.

Abbreviations

C/N, carbon to nitrogen ratio; DOE, dissolved oxygen efficiency; DEM, discrete element method; RSM, response surface methodology; RS, rotary drum reactor speed; RA, rotary drum reactor horizontal angle of inclination; BA, mixing blade angle of inclination; BP, blade pitch; FEM, finite element method; FW, food waste; UNEP, United Nations Environment Programme; CFD, computational fluid dynamics; SLs, sycamore leaves; MSM, multisphere method; SV, strain variable; BBD, Box–Behnken experimental design; VD, volumetric density; GI, seed germination index; HS, humic substance; HA, humic acid; FA, fulvic acid; CV, coefficient of variation; R^2, correlation coefficient; RSA, response surface analysis; FEA, finite element analysis.

References

1. Hermanussen, H.; Loy, J.-P. Household food waste: A meta-analysis. *Environ. Chall.* **2024**, *14*, 100809. [CrossRef]
2. Hossain, M.S.; Das, B.K.; Das, A.; Roy, T.K. Investigating the techno-economic and environmental feasibility of biogas-based power generation potential using food waste in Bangladesh. *Renew. Energy* **2024**, *232*, 121017. [CrossRef]
3. Ayilara, M.S.; Olanrewaju, O.S.; Babalola, O.O.; Odeyemi, O. Waste Management through Composting: Challenges and Potentials. *Sustainability* **2020**, *12*, 4456. [CrossRef]
4. Zhang, Z.; Li, X.; Hu, X.; Zhang, S.; Li, A.; Deng, Y.; Wu, Y.; Li, S.; Che, R.; Cui, X. Downward aeration promotes static composting by affecting mineralization and humification. *Bioresour. Technol.* **2021**, *338*, 125592. [CrossRef] [PubMed]
5. Liu, T.; Ren, X.; Zhao, J.; Chen, H.; Wang, Q.; Awasthi, S.K.; Duan, Y.; Pandey, A.; Taherzadeh, M.J.; Awasthi, M.K. Sustainability analysis of large-scale food waste composting. In *Current Developments in Biotechnology and Bioengineering*; Elsevier: Amsterdam, The Netherlands, 2020; pp. 301–322.
6. Sharma, D.; Saadi, I.; Oazana, S.; Lati, R.; Laor, Y. Distribution of residence time in rotary-drum composting and implications for hygienization. *Waste Manag.* **2024**, *179*, 22–31. [CrossRef]
7. Sayara, T.; Shadouf, M.; Issa, H.; Obaid, H.; Hanoun, R. Home composting of food wastes using rotary drum reactor as an alternative treatment option for organic household wastes. *J. Ecol. Eng.* **2022**, *23*, 139–147. [CrossRef]
8. Rodriguez, L.; Cerrillo, M.I.; Garcia-Albiach, V.; Villasenor, J. Domestic sewage sludge composting in a rotary drum reactor: Optimizing the thermophilic stage. *J. Environ. Manag.* **2012**, *112*, 284–291. [CrossRef]
9. Nayak, A.K.; Kalamdhad, A.S. Feasibility of Composting Combinations of Sewage Sludge, Cattle Manure, and Sawdust in a Rotary Drum Reactor. *Environ. Eng. Res.* **2014**, *19*, 47–57. [CrossRef]
10. Anwar, Z.; Gulfraz, M.; Irshad, M. Agro-industrial lignocellulosic biomass a key to unlock the future bio-energy: A brief review. *J. Radiat. Res. Appl. Sci.* **2014**, *7*, 163–173. [CrossRef]
11. Soysal, A.; Demirciolu, P.; Breki, S. *Improvement of Solid Spreader Blade Design Using Discrete Element Method (DEM) Applications*; Springer: Berlin/Heidelberg, Germany, 2022.

12. Wang, J.; Li, C.; Zhu, Z.; Zhu, X.; Li, H.; Nyambura, S.M.; Feng, X.; Zhou, H. Bionic stirring device for horizontal composter to improve aeration efficiency: Design and optimisation using discrete and finite element methods. *Comput. Electron. Agric.* **2024**, *225*, 109257. [CrossRef]

13. Prommuak, C.; Jarunglumlert, T.; Putmai, N.; Sawatdee, S.; Sanguanwong, A.; Pavasant, P. Comparative study on different turning device alignments for household food waste composters. *Environ. Prog. Sustain. Energy* **2018**, *37*, 1954–1958. [CrossRef]

14. Liu, Y.; Wang, X.; Sun, Y. Optimization and experimental study of variable frequency intermittent stirring strategy for anaerobic digestion based on CFD. *Fuel* **2024**, *355*, 129371. [CrossRef]

15. Wang, J.; Li, C.; Awasthi, M.K.; Nyambura, S.M.; Zhu, Z.; Li, H.; Xu, J.; Feng, X.; Zhu, X.; Syed, A. Utilising standard samples instead of randomly collected food waste in composting: Implementation strategy and feasibility evaluation. *J. Environ. Manag.* **2024**, *353*, 120182. [CrossRef]

16. Zhao, K.; Xu, R.; Zhang, Y.; Tang, H.; Zhou, C.; Cao, A.; Zhao, G.; Guo, H. Development of a novel compound microbial agent for degradation of kitchen waste. *Braz. J. Microbiol.* **2017**, *48*, 442–450. [CrossRef]

17. Chen, X.; Cheng, W.; Li, S.; Tang, X.; Wei, Z. The "quality" and "quantity" of microbial species drive the degradation of cellulose during composting. *Bioresour. Technol.* **2021**, *320*, 124425. [CrossRef]

18. Mishra, S.K.; Yadav, K.D. Assessment of the effect of particle size and selected physico-chemical and biological parameters on the efficiency and quality of composting of garden waste. *J. Environ. Chem. Eng.* **2022**, *10*, 107925. [CrossRef]

19. Cheng, J.; Gao, X.; Yan, Z.; Li, G.; Luo, W.; Xu, Z. Intermittent aeration to reduce gaseous emission and advance humification in food waste digestate composting: Performance and mechanisms. *Bioresour. Technol.* **2023**, *371*, 128644. [CrossRef] [PubMed]

20. Peng, T.; Yue, S.; Mao, W.; Yang, Q.; Jiang, G. Preparation of high-temperature and low-temperature-resistant solid microbial agent for cattle manure fermentation and effect on composting. *Environ. Sci. Pollut. Res.* **2024**, *31*, 29017–29032. [CrossRef]

21. Peng, L.; Ma, R.; Jiang, S.; Luo, W.; Li, Y.; Wang, G.; Xu, Z.; Wang, Y.; Qi, C.; Li, Y. Co-composting of kitchen waste with agriculture and forestry residues and characteristics of compost with different particle size: An industrial scale case study. *Waste Manag.* **2022**, *149*, 313–322. [CrossRef]

22. Wang, X.; Pan, S.; Zhang, Z.; Lin, X.; Zhang, Y.; Chen, S. Effects of the feeding ratio of food waste on fed-batch aerobic composting and its microbial community. *Bioresour. Technol.* **2017**, *224*, 397–404. [CrossRef]

23. Zhu, H.; Wang, D.; He, X.; Shang, S.; Zhao, Z.; Wang, H.; Tan, Y.; Shi, Y. Study on plant crushing and soil throwing performance of bionic rotary blades in Cyperus esculentus harvesting. *Machines* **2022**, *10*, 562. [CrossRef]

24. Yuan, J.; Wang, J.; Li, H.; Qi, X.; Wang, Y.; Li, C. Optimization of the cylindrical sieves for separating threshed rice mixture using EDEM. *Int. J. Agric. Biol. Eng.* **2022**, *15*, 236–247. [CrossRef]

25. Sadasivuni, K.K.; Saha, P.; Adhikari, J.; Deshmukh, K.; Ahamed, M.B.; Cabibihan, J.J. Recent advances in mechanical properties of biopolymer composites: A review. *Polym. Compos.* **2020**, *41*, 32–59. [CrossRef]

26. Sumesh, K.; Kanthavel, K. Abrasive water jet machining of Sisal/Pineapple epoxy hybrid composites with the addition of various fly ash filler. *Mater. Res. Express* **2020**, *7*, 035303. [CrossRef]

27. Hsu, Y.-C.; Gung, Y.-W.; Shih, S.-L.; Feng, C.-K.; Wei, S.-H.; Yu, C.-h.; Chen, C.-S. Using an optimization approach to design an insole for lowering plantar fascia stress—A finite element study. *Ann. Biomed. Eng.* **2008**, *36*, 1345–1352. [CrossRef]

28. Choi, I.; Corson, N.; Peiros, L.; Hawkes, E.W.; Keller, S.; Follmer, S. A soft, controllable, high force density linear brake utilizing layer jamming. *IEEE Robot. Autom. Lett.* **2017**, *3*, 450–457. [CrossRef]

29. Chuang, Y.-C.; Li, T.-T.; Huang, C.-H.; Huang, C.-L.; Lou, C.-W.; Chen, Y.-S.; Lin, J.-H. Protective rigid fiber-reinforced polyurethane foam composite boards: Sound absorption, drop-weight impact and mechanical properties. *Fibers Polym.* **2016**, *17*, 2116–2123. [CrossRef]

30. Gamble, S.; Coker, C.S.; Franciosi, F.; Rynk, R. Composting operations and equipment. In *The Composting Handbook*; Elsevier: Amsterdam, The Netherlands, 2022; pp. 341–408.

31. Alkoaik, F.N.; Abdel-Ghany, A.M.; Rashwan, M.A.; Fulleros, R.B.; Ibrahim, M.N. Energy analysis of a rotary drum bioreactor for composting tomato plant residues. *Energies* **2018**, *11*, 449. [CrossRef]

32. Cheng, H.S.; Sui, B.; Meng, H.; Shen, Y.; Wang, J.; Kuang, C. Design and performance test of aerobic fermentation rotary reactor pilot plant for biogas residue. *Trans. Chin. Soc. Agric. Eng.* **2018**, *34*, 8.

33. Mahdavy, S.; Norouzi, H.R.; Jordan, C.; Haddadi, B.; Harasek, M. Residence Time Distribution of Non-Spherical Particles in a Continuous Rotary Drum. *Processes* **2022**, *10*, 1069. [CrossRef]

34. Fudin, K.; Konovalov, V.; Zaitsev, V. Regression Dependence of the Influence of the Installation Angles of Drum Mixer Blades on the Quality of Mixture. *IOP Conf. Ser. Mater. Sci. Eng.* **2021**, *1079*, 072003. [CrossRef]

35. Niță, A.; Laudacescu, E.; Petrescu, M.G.; Dumitru, T.; Burlacu, A.; Bădoiu, D.G.; Tănase, M. Experimental Research Regarding the Effect of Mineral Aggregates on the Wear of Mixing Blades of Concrete Mixers. *Materials* **2023**, *16*, 5047. [CrossRef]

36. Gao, S.; Meng, L.; Zhou, X.; Shen, Y.; Cui, B.; Song, Z. Design of partial cross-sectional geometry and prediction of separation performance in the spiral separator. *Sep. Sci. Technol.* **2022**, *57*, 2127–2144. [CrossRef]

37. Adah, E.; Joubert, A.; Henry, M.; Durécu, S.; Le Coq, L. Optimization of Nanoparticle Collection by a Pilot-Scale Spray Scrubber Operated Under Waste Incineration Conditions: Using Box–Behnken Design. *Waste Biomass Valorization* **2023**, *14*, 3455–3474. [CrossRef]

38. Asadu, C.O.; Egbuna, S.O.; Chime, T.O.; Eze, C.N.; Kevin, D.; Mbah, G.O.; Ezema, A.C. Survey on solid wastes management by composting: Optimization of key process parameters for biofertilizer synthesis from agro wastes using response surface methodology (RSM). *Artif. Intell. Agric.* **2019**, *3*, 52–61. [CrossRef]

39. Du, B.; Zhao, C.; Dong, G.; Bi, J. FEM-DEM coupling analysis for solid granule medium forming new technology. *J. Mater. Process. Technol.* **2017**, *249*, 108–117. [CrossRef]

40. Mazor, A.; Orefice, L.; Michrafy, A.; De Ryck, A.; Khinast, J.G. A combined DEM & FEM approach for modelling roll compaction process. *Powder Technol.* **2018**, *337*, 3–16.

41. Chen, G.; Wang, Q.; Xu, D.; Li, H.; He, J.; Lu, C. Design and experimental research on the counter roll differential speed solid organic fertilizer crusher based on DEM. *Comput. Electron. Agric.* **2023**, *207*, 107748. [CrossRef]

42. Albrecht, R.; Le Petit, J.; Terrom, G.; Périssol, C. Comparison between UV spectroscopy and nirs to assess humification process during sewage sludge and green wastes co-composting. *Bioresour. Technol.* **2011**, *102*, 4495–4500. [CrossRef]

43. Wang, G.; Yang, Y.; Kong, Y.; Ma, R.; Yuan, J.; Li, G. Key factors affecting seed germination in phytotoxicity tests during sheep manure composting with carbon additives. *J. Hazard. Mater.* **2022**, *421*, 126809. [CrossRef]

44. Wang, J.; Li, C.; Nyambura, S.M.; Xu, J.; Li, H.; Geng, C.; Li, X.; Feng, X.; Zhu, X. Co-pyrolysis of food waste with coconut fiber: Thermogravimetric analyzes and hydrogen yield optimization. *Energy Sources Part A Recovery Util. Environ. Eff.* **2022**, *44*, 10230–10247. [CrossRef]

45. Pélabon, C.; Hilde, C.H.; Einum, S.; Gamelon, M. On the use of the coefficient of variation to quantify and compare trait variation. *Evol. Lett.* **2020**, *4*, 180–188. [CrossRef]

46. Edward, A.B.; Heyns, P.S.; Kok, S. A numerical investigation of a single-shot in a DEM-FEM approach to shot peening simulation. *Metals* **2019**, *9*, 1183. [CrossRef]

47. Zhao, G.; Pu, K.; Xu, N.; Gong, S.; Wang, X. Simulation of particles motion on a double vibrating flip-flow screen surface based on FEM and DEM coupling. *Powder Technol.* **2023**, *421*, 118422. [CrossRef]

48. Du, Y.; Zhou, S.; Jing, X.; Peng, Y.; Wu, H.; Kwok, N. Damage detection techniques for wind turbine blades: A review. *Mech. Syst. Signal Process.* **2020**, *141*, 106445. [CrossRef]

49. Verma, D.; Kainthola, A.; Gupte, S.; Singh, T. A finite element approach of stability analysis of internal dump slope in Wardha valley coal field, India, Maharashtra. *Am. J. Min. Metall.* **2013**, *1*, 1–6.

50. Bulan, R.; Rahmah, R.; Hasan, A.R.; Sitorus, A. Design and construction of oil palm fronds (OPF) compost mixer machine type rotary double helix drum. In Proceedings of the 2019 5th International Conference on Computing Engineering and Design (ICCED), Singapore, 11–13 April 2019; pp. 1–4.

51. Palaniveloo, K.; Amran, M.; Norhashim, N.; Mohamad-Fauzi, N.; Peng-Hui, F.; Hui-Wen, L.; Kai-Lin, Y.; Jiale, L.; Chian-Yee, M.; Jing-Yi, L. Food waste composting and microbial community structure profiling. *Processes* **2020**, *8*, 723. [CrossRef]

52. Partanen, P.; Hultman, J.; Paulin, L.; Auvinen, P.; Romantschuk, M. Bacterial diversity at different stages of the composting process. *BMC Microbiol.* **2010**, *10*, 94. [CrossRef]

53. Zhang, W.; Yu, C.; Wang, X.; Hai, L. Increased abundance of nitrogen transforming bacteria by higher C/N ratio reduces the total losses of N and C in chicken manure and corn stover mix composting. *Bioresource Technology* **2020**, *297*, 122410. [CrossRef]

54. Shridhar, B.S. Nitrogen fixing microorganisms. *Int. J. Microbiol. Res.* **2012**, *3*, 46–52.

55. Påledal, S.N.; Hellman, E.; Moestedt, J. The effect of temperature, storage time and collection method on biomethane potential of source separated household food waste. *Waste Manag.* **2018**, *71*, 636–643. [CrossRef] [PubMed]

56. Jiang, F.-G.; Cheng, H.-J.; Liu, D.; Wei, C.; An, W.-J.; Wang, Y.-F.; Sun, H.-T.; Song, E.-L. Treatment of Whole-Plant Corn Silage With Lactic Acid Bacteria and Organic Acid Enhances Quality by Elevating Acid Content, Reducing pH, and Inhibiting Undesirable Microorganisms. *Front. Microbiol.* **2020**, *11*, 93088. [CrossRef] [PubMed]

57. Rees, D.C.; Akif Tezcan, F.; Haynes, C.A.; Walton, M.Y.; Andrade, S.; Einsle, O.; Howard, J.B. Structural basis of biological nitrogen fixation. *Philos. Trans. R. Soc. A Math. Phys. Eng. Sci.* **2005**, *363*, 971–984. [CrossRef]

58. Guo, X.-X.; Liu, H.-T.; Wu, S.-B. Humic substances developed during organic waste composting: Formation mechanisms, structural properties, and agronomic functions. *Sci. Total Environ.* **2019**, *662*, 501–510. [CrossRef]

59. Cheng, K.H.; Huang, M.C.; Lu, M.F.; Chou, Y.J.; Lin, J.J.M. Assessment of degree of maturity of compost produced by different kitchen waste composting methods. *Adv. Mater. Res.* **2013**, *652*, 1642–1651. [CrossRef]

60. Huang, G.F.; Wong, J.; Wu, Q.; Nagar, B. Effect of C/N on composting of pig manure with sawdust. *Waste Manag.* **2004**, *24*, 805–813. [CrossRef]

61. Li, Z.; Huang, G.; Yu, H.; Zhou, Y.; Huang, W. Critical factors and their effects on product maturity in food waste composting. *Environ. Monit. Assess.* **2015**, *187*, 217. [CrossRef]

62. Li, H.; Li, Y.; Li, C. Evolution of humic substances during anaerobic sludge digestion. *Environ. Eng. Manag. J. (EEMJ)* **2017**, *16*, 1577–1582. [CrossRef]

63. Awasthi, M.K.; Selvam, A.; Chan, M.T.; Wong, J.W. Bio-degradation of oily food waste employing thermophilic bacterial strains. *Bioresour. Technol.* **2018**, *248*, 141–147. [CrossRef]

64. Piccolo, A.; Spaccini, R.; Drosos, M.; Vinci, G.; Cozzolino, V. The molecular composition of humus carbon: Recalcitrance and reactivity in soils. In *The future of Soil Carbon*; Elsevier: Amsterdam, The Netherlands, 2018; pp. 87–124.

65. Wang, G.; Li, G.; Chang, J.; Kong, Y.; Jiang, T.; Wang, J.; Yuan, J. Enrichment of antibiotic resistance genes after sheep manure aerobic heap composting. *Bioresour. Technol.* **2021**, *323*, 124620. [CrossRef]